Fano-Andreev effect in a parallel double quantum dot structure

Xiao-Qi Wang,[1] Shu-Feng Zhang,[2] Yu Han,[3] and Wei-Jiang Gong[1,*]
[1]*College of Sciences, Northeastern University, Shenyang 110819, China*
[2]*School of Physics and Technology, University of Jinan, Jinan, Shandong 250022, China*
[3]*School of Physics, Liaoning University, Shenyang 110036, China*

(Received 18 December 2018; revised manuscript received 16 May 2019; published 4 September 2019)

We investigate the Andreev reflection in a parallel double quantum dot structure, by considering one metallic lead coupled to one *s*-wave superconductor through the quantum dots. It is found that if an arm of this system provides the reference channel for the Andreev reflection, the Fano line shapes will have opportunities to appear in the linear conductance spectra and can be reversed by adjusting the dot level or local magnetic flux. To present the underlying physics, we obtain the Fano form of the linear conductance expression. Despite the complicated structural parameters, the property of the Fano effect is clearly shown. We believe that the results of this work will help us to understand the Fano interference in the Andreev reflection process.

DOI: 10.1103/PhysRevB.100.115405

I. INTRODUCTION

The Fano effect, well known for the asymmetric line shapes in the spectra concerned, is an important phenomenon in many physics fields, such as optics, atom and molecule physics, and condensed matter physics. It originates from the interference between resonance and reference processes [1]. In low-dimensional semiconductor systems, electronic transport is governed by quantum coherence. As the resonant and nonresonant tunneling channels are achieved, the Fano line shapes can appear in the transport spectra [2]. A typical system for observing the Fano effect is the coupled quantum dot (QD) structure, which provides multiple channels for electronic coherent transmission. In the appropriate parameter region, one or several channels serve as the resonant paths for electron tunneling while the others are nonresonant, which accordingly lead to the occurrence of Fano interference [3].

The Fano effect manifests itself in QD structures by the experimental observation of the asymmetric line shapes in the conductance spectra [4–9]. Relevant theoretical investigations involve various structures, for example, one or two QDs embedded in an Aharonov-Bohm ring [10–16], or the double QDs in different coupling manners [17–21]. According to their results, the Fano effect in the QD structures exhibits peculiar behaviors in the electronic transport process, in contrast to the conventional Fano effect. These include the tunable Fano line shape by the magnetic or electrostatic fields applied on the QDs [17–20], the Kondo resonance associated Fano effect [10,11,21], Coulomb modification of the Fano effect [22], the spin-dependent Fano effect [23], and the relation between the dephasing time and the Fano parameter q [24]. In addition, the Fano effect has been demonstrated to help improve the thermoelectric efficiency [25].

At the same time, the developments of the microfabrication technology has promoted scientists to become interested in the mesoscopic systems with the coexistence of normal metals and superconductors (SCs) [26–32]. It is known that in such systems, the so-called Andreev reflection (AR) is allowed to take place at the metal-SC interface due to the appearance of a new energy scale, i.e., the superconducting pairing energy Δ [33]. This phenomenon can be described as follows. If an electron from the normal metal is injected into the SC, it will be reflected as a hole, thereby transferring a Cooper pair into the SC. Furthermore, when the coupled QDs are embedded between the normal metal and SC, intricate phenomena can be observed, e.g., the appearance of Shiba states, due to the effect of abundant quantum interference [34]. Since the SC is a natural source of the entanglement electrons, the multiterminal hybrid systems have been proposed to be promising candidates for the Cooper-pair splitting [35], when the crossed AR between the normal metals is enhanced [36,37].

Following research progress in the above two aspects, the Fano effect in the AR process has attracted extensive attentions [38–46]. And some interesting phenomena have been observed. Peng *et al.* discuss the AR in a four-QD Aharonov-Bohm interferometer, and they find that in this system, the reciprocity relation of conductance $\mathcal{G}(\varphi) = \mathcal{G}(-\varphi)$ holds. Moreover, the antiresonance point appears in the AR conductance spectrum with the adjustment of the systematic parameters [40]. For the parallel-coupled double QDs with spin-flip scattering, the Fano resonance has also been observed though it is relatively weak. And the spin-flip scattering enables us to induce the splitting of the Fano peak [41]. Other groups have reported the AR in a normal metal-molecule-SC junction using the first-principles approach. They demonstrate that the presence of the side group in the molecule can lead to a Fano resonance in the AR process [42]. In addition, it has been shown that when the T-shaped double QDs are inserted in the metal-SC junction, two separate Fano structures appear in the gate-voltage dependence of the AR process [43]. When an additional terminal is introduced, decoherence has its effects on the Fano line shapes in the T-shaped double QDs coupled between the metal and SC [44]. These results

*Corresponding author: gwj@mail.neu.edu.cn

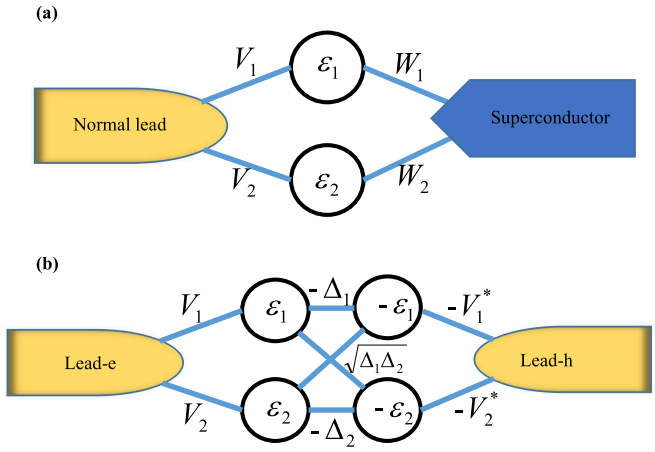

FIG. 1. (a) Schematic of one parallel double QD structure. In this geometry, the QDs are coupled to one normal metallic lead and one *s*-wave SC simultaneously. (b) Illustration of our considered structure in the Nambu representation for the infinite superconducting pairing potential in the SC.

do indicate that the Fano effect in the AR process is very interesting. However, in order to completely clarify its physics picture, further discussions are still necessary.

In the present work we aim to investigate the Fano interference in the AR of the parallel double QD structure, by supposing a metallic lead to couple to a SC via the QDs. The numerical results show that the AR spectra are tightly related to the structural parameters and the threaded magnetic flux. The obvious phenomenon is that the Fano line shapes will appear in the linear AR conductance spectra, and they can also be reversed by adjusting the QD level and local magnetic flux. However, we observe that the Fano resonance conditions are completely different from those in the normal electron transport cases [47]. Therefore, the results in this work provide useful information for describing the Fano interference in the AR process.

The rest of this paper is organized as follows. In Sec. II the model Hamiltonian for describing the electron motion in the parallel double QD structure is first introduced. The formula for the linear AR conductance is then derived by means of the nonequilibrium Green function technique. In Sec. III the calculated results about the linear conductance spectra are shown. Then discussions focusing on the formation of the Fano line shapes are given. Finally, the main results are summarized in Sec. IV.

II. MODEL

The parallel double QD structure that we consider is illustrated in Fig. 1, in which two QDs are inserted in the AR heterostructure formed by the normal metal and SC in the parallel way. It can be certain that the AR in this system is dependent on the quantum interference. The Hamiltonian that describes the electronic motion in this double QD geometry reads

$$H = H_n + H_s + H_d + H_{nT} + H_{sT}. \tag{1}$$

The first two terms (i.e., H_n and H_s) are the Hamiltonians for the electrons in the normal metallic lead and SC, respectively:

$$H_n = \sum_{k\sigma} \varepsilon_k c^\dagger_{k\sigma} c_{k\sigma},$$
$$H_s = \sum_{k\sigma} \epsilon_k a^\dagger_{k\sigma} a_{k\sigma} + \sum_k (\Delta_k a^\dagger_{k\uparrow} a^\dagger_{-k\downarrow} + \text{H.c.}). \tag{2}$$

$c^\dagger_{k\sigma}$ ($c_{k\sigma}$) is an operator to create (annihilate) an electron of the continuous state $|k\sigma\rangle$ in the normal metallic lead, and ε_k is the corresponding single-particle energy. $a^\dagger_{k\sigma}$ ($a_{k\sigma}$) is the creation (annihilation) operator in the SC. ϵ_k denotes the corresponding energy, and Δ_k is the superconducting pairing potential.

The third term describes the electron in the double QDs. It takes the form as

$$H_d = \sum_{\sigma,j=1}^{2} \varepsilon_j d^\dagger_{j\sigma} d_{j\sigma}, \tag{3}$$

where $d^\dagger_{j\sigma}$ ($d_{j\sigma}$) is the creation (annihilation) operator of the spin-σ electron in the jth QD, and ε_j denotes the corresponding electron level. We here assume that only one level is relevant in each QD, since we are mainly interested in the AR governed by the quantum coherence. Also, in order to investigate the leading AR properties governed by the quantum interference, the Coulomb terms have been ignored. The last two terms in the Hamiltonian denote the QD-lead and QD-SC couplings. They are given by

$$H_{nT} = \sum_{k\sigma,j} V_{jk} d^\dagger_{j\sigma} c_{k\sigma} + \text{H.c.},$$
$$H_{sT} = \sum_{k\sigma,j} W_{jk} d^\dagger_{j\sigma} a_{k\sigma} + \text{H.c.} \tag{4}$$

V_{jk} (W_{jk}) corresponds to the QD-lead (QD-SC) coupling strength with $j = 1, 2$. Since a quantum ring is formed in this geometry, local magnetic flux can be introduced to modulate the quantum interference. In such a case, finite phase shift will attach to the QD-lead coupling coefficients, which gives that $V_{1k} = |V_{1k}|e^{-i\varphi/2}$ and $V_{2k} = |V_{2k}|e^{i\varphi/2}$. The phase shift φ is associated with the magnetic flux Φ threading the system by a relation $\varphi = 2\pi\Phi/\Phi_0$, in which $\Phi_0 = h/e$ is the flux quantum [3,48].

In this work we concentrate on the AR process in the superconducting gap, hence the approximation of $\Delta_k \to \infty$ is feasible [49,50]. It should be emphasized that in such a case, as the Bogoliubov quasiparticle in the SC is inaccessible, tracing out of the degree of freedom of the SC does not induce any dissipative dynamics in the QD system and it can be performed exactly. The resulting dynamics process of the considered structure can be reexpressed by the following effective Hamiltonian: $H = H_n + \tilde{H}_d + H_{nT}$, where

$$\tilde{H}_d = \sum_{\sigma,j=1}^{2} \varepsilon_j d^\dagger_{j\sigma} d_{j\sigma} - \sum_{j=1}^{2} \Delta_j d^\dagger_{j\uparrow} d^\dagger_{j\downarrow} + \sqrt{\Delta_1\Delta_2} d^\dagger_{1\uparrow} d^\dagger_{2\downarrow}$$
$$+ \sqrt{\Delta_1\Delta_2} d^\dagger_{2\uparrow} d^\dagger_{1\downarrow} + \text{H.c.} \tag{5}$$

Δ_j, defined by $\Delta_j = \pi \sum_k |W_{jk}|^2 \delta(\omega - \epsilon_k)$, represents the effective superconducting pairing potential in QD-j induced

by the proximity effect between the SC and it. The more interesting contribution is the third and fourth terms, which describe the formation of nonlocal superconducting correlations between the two QDs. They exactly encompass the Cooper-pair splitting in the double QD system. In fact, the above effective Hamiltonian can be obtained by adding up all contributions in Δ_j within a real-time perturbative expansion [51,52]. In Appendix A we also present the derivation for convenience.

According to the new form of H, we next proceed to calculate the current passing through the metallic lead, which can be defined as $J=-e\langle\dot{\hat{N}}\rangle$ with $\hat{N}=\sum_{k\sigma}c^{\dagger}_{k\sigma}c_{k\sigma}$. Using the Heisenberg equation of motion, the current can be rewritten as $J=-e\sum_{j,k\sigma}[V_{jk}G^{<}_{jk,\sigma}(t,t)+\text{c.c.}]$, where $G^{<}_{jk,\sigma}(t,t')=i\langle c^{\dagger}_{k\sigma}(t')d_{j\sigma}(t)\rangle$ is the lesser Green's function. With the help of the Langreth continuation theorem and the Fourier transformation, we have [53]

$$J=\frac{e}{h}\int dE\,\mathrm{Tr}\{\sigma_3\Gamma[(G^r-G^a)f(E)+G^{<}]\} \tag{6}$$

in which $f(E)$ is the Fermi distribution function and σ_3 is the Pauli matrix. $G^{r,a,<}$ are the retarded, advanced, and lesser Green's functions in the Nambu representation, which are defined as $G^r(t,t')=-i\theta(t-t')\langle\{\Psi(t),\Psi^{\dagger}(t')\}\rangle$ and $G^{<}(t,t')=i\langle\{\Psi^{\dagger}(t')\Psi(t)\}\rangle$ with $G^a=[G^r]^{\dagger}$. The field operator involved, i.e., Ψ, is given by $\Psi=[d_{1\uparrow},d^{\dagger}_{1\downarrow},d_{2\uparrow},d^{\dagger}_{2\downarrow}]^T$. Γ is the linewidth matrix function of the metallic lead, which describes the coupling strength between the lead and the QDs. If the lead is manufactured by the two-dimensional electron gas, the elements of Γ will be independent of energy.

It is not difficult to find that for calculating the current, one must obtain the expressions of the retarded and lesser Green's functions. The retarded Green's function can be in principle deduced from the Dyson's equation. Via a straightforward derivation, the matrix of the retarded Green's function can be written out, i.e.,

$$[G^r(E)]^{-1}=\begin{bmatrix} g_{1e}(E)^{-1} & \Delta_1 & \frac{i}{2}\Gamma_{12,e} & -\sqrt{\Delta_1\Delta_2} \\ \Delta_1 & g_{1h}(E)^{-1} & -\sqrt{\Delta_1\Delta_2} & \frac{i}{2}\Gamma_{12,h} \\ \frac{i}{2}\Gamma_{21,e} & -\sqrt{\Delta_1\Delta_2} & g_{2e}(E)^{-1} & \Delta_2 \\ -\sqrt{\Delta_1\Delta_2} & \frac{i}{2}\Gamma_{21,h} & \Delta_2 & g_{2h}(E)^{-1} \end{bmatrix}, \tag{7}$$

where $g_{je(h)}=[E\mp\varepsilon_j+\frac{i}{2}\Gamma_{jj,e}]^{-1}$. $\Gamma_{jl,e}$ and $\Gamma_{jl,h}$ are defined as $\Gamma_{jl,e}=2\pi\sum_k V_{jk}V^{*}_{lk}\delta(E-\varepsilon_k)$ and $\Gamma_{jl,h}=2\pi\sum_k V^{*}_{jk}V_{lk}\delta(E+\varepsilon_k)$, respectively. Note that because of spin degeneracy, we here only choose the basis of $\{\phi_{1e\uparrow},\phi_{1h\downarrow},\phi_{2e\uparrow},\phi_{2h\downarrow}\}$. Within the wide-band approximation of the lead, we will have $\Gamma_{jj,e}=\Gamma_{jj,h}$. And then, the matrices of Γ_e and Γ_h can respectively be expressed as

$$\Gamma_e=\begin{bmatrix} \Gamma_1 & 0 & \sqrt{\Gamma_1\Gamma_2}e^{-i\varphi} & 0 \\ 0 & 0 & 0 & 0 \\ \sqrt{\Gamma_1\Gamma_2}e^{i\varphi} & 0 & \Gamma_2 & 0 \\ 0 & 0 & 0 & 0 \end{bmatrix} \tag{8}$$

and

$$\Gamma_h=\begin{bmatrix} 0 & 0 & 0 & 0 \\ 0 & \Gamma_1 & 0 & \sqrt{\Gamma_1\Gamma_2}e^{i\varphi} \\ 0 & 0 & 0 & 0 \\ 0 & \sqrt{\Gamma_1\Gamma_2}e^{-i\varphi} & 0 & \Gamma_2 \end{bmatrix}. \tag{9}$$

As for the lesser Green's function, it can be solved using the Keldysh equation $G^{<}=G^r\Sigma^{<}G^a$, where

$$\Sigma^{<}=\begin{bmatrix} \Sigma^{<}_{11} & \Sigma^{<}_{12} \\ \Sigma^{<}_{21} & \Sigma^{<}_{22} \end{bmatrix} \tag{10}$$

with $\Sigma^{<}_{jl}=\begin{bmatrix} i\Gamma_{jl,e}f(E-eV) & 0 \\ 0 & i\Gamma_{jl,h}f(E+eV) \end{bmatrix}$. Based on the derivation above, the electronic current is further simplified, i.e.,

$$J=\frac{2e}{h}\int dE\{T_A(E)[f(E-eV)-f(E+eV)]\}, \tag{11}$$

where $T_A=\mathrm{Tr}[\Gamma_eG^r(E)\Gamma_hG^a(E)]$ is the AR transmittance. At the case of zero temperature limit, the current formula can be reexpressed, yielding $J=\frac{2e}{h}\int_{-eV}^{eV}T_A(E)dE$.

It is evident that $T_A(E)$ is the most critical quantity to evaluate the electronic current driven by the AR. In the noninteracting case, we are allowed to write out its analytical expression. One direct method is to define $T_A(E)=|\tau(E)|^2=|\sum_{jl}\tau_{jl}|^2$ with

$$\begin{aligned} &\tau_{11}=\Gamma_1G^r_{12}e^{i\varphi},\quad \tau_{12}=\sqrt{\Gamma_1\Gamma_2}G^r_{14}, \\ &\tau_{21}=\sqrt{\Gamma_1\Gamma_2}G^r_{32},\quad \tau_{22}=\Gamma_2G^r_{34}e^{-i\varphi}. \end{aligned} \tag{12}$$

Via solving the Green's functions in Eq. (7) (see Appendix B), the AR coefficient can be expressed, i.e.,

$$\tau(E)=\frac{E^2(e^{-i\varphi}\Gamma_2\Delta_2+e^{i\varphi}\Gamma_1\Delta_1-2\sqrt{\Gamma_1\Gamma_2\Delta_1\Delta_2})-\left(e^{-i\frac{\varphi}{2}}\varepsilon_1\sqrt{\Gamma_2\Delta_2}-e^{i\frac{\varphi}{2}}\varepsilon_2\sqrt{\Gamma_1\Delta_1}\right)^2}{\det|[G^r(E)]^{-1}|}. \tag{13}$$

At the zero-bias limit, we will have $J=\mathcal{G}\cdot V$ with the linear AR conductance given by

$$\mathcal{G}=\frac{4e^2}{h}T_A|_{E=0}. \tag{14}$$

Note that at equilibrium, the chemical potential in the normal metallic lead has been assumed to be zero. As a result, the expression of $\tau|_{E=0}$ is written as

$$\tau|_{E=0}=\frac{-4\left(e^{-i\frac{\varphi}{2}}\varepsilon_1\sqrt{\Gamma_2\Delta_2}-e^{i\frac{\varphi}{2}}\varepsilon_2\sqrt{\Gamma_1\Delta_1}\right)^2}{(\varepsilon_1\Gamma_2+\varepsilon_2\Gamma_1)^2+4(\varepsilon_1\Delta_2+\varepsilon_2\Delta_1)^2+4\varepsilon_1^2\varepsilon_2^2+\mathcal{C}}, \tag{15}$$

where $\mathcal{C} = |\sqrt{\Gamma_1\Delta_2}e^{i\varphi/2} + \sqrt{\Gamma_2\Delta_1}e^{-i\varphi/2}|^4$. For the case of $\Delta_j = \Delta$, there will be

$$\tau|_{E=0} = \frac{-4\Delta\left(e^{-i\frac{\varphi}{2}}\varepsilon_1\sqrt{\Gamma_2} - e^{i\frac{\varphi}{2}}\varepsilon_2\sqrt{\Gamma_1}\right)^2}{(\varepsilon_1\Gamma_2 + \varepsilon_2\Gamma_1)^2 + 4\Delta^2(\varepsilon_1+\varepsilon_2)^2 + 4\varepsilon_1^2\varepsilon_2^2 + \mathcal{C}} \quad (16)$$

in which $\mathcal{C} = \Delta^2|\sqrt{\Gamma_1}e^{i\varphi/2} + \sqrt{\Gamma_2}e^{-i\varphi/2}|^4$. All these results can help us to complete the investigation about the AR in this structure.

III. NUMERICAL RESULTS AND DISCUSSIONS

With the help of the formulations developed in Sec. II, we continue to perform calculations to investigate the AR in the parallel double QD structure with one coupled SC. To do so, we would like to consider two typical coupling manners, i.e., the case of symmetric QD-lead(SC) coupling where $\Gamma_j = \Gamma$ and $\Delta_j = \Delta$ and the case of asymmetric QD-lead(SC) coupling where $\Gamma_1 = \lambda\Gamma_2$ and $\Delta_1 = \lambda\Delta_2$ with $\lambda > 1$.

A. Case of symmetric QD-lead(SC) couplings

We first choose the case of symmetric QD-lead(SC) coupling and present the AR spectra of the parallel double QD structure. In such a case, the AR coefficient in Eq. (13) can be written directly, i.e.,

$$\tau(E) = \frac{(2\cos\varphi - 2)E^2 - (e^{-i\varphi/2}\varepsilon_1 - e^{i\varphi/2}\varepsilon_2)^2}{\det|[G^r(E)]^{-1}|}\Gamma\Delta. \quad (17)$$

It will be transformed into $\tau(E) = \frac{-(\varepsilon_1-\varepsilon_2)^2}{\det|[G^r(E)]^{-1}|}\Gamma\Delta$, in the absence of magnetic flux. This means that the antiresonance points appear at the positions of $\varepsilon_1 = \varepsilon_2$ in the AR spectrum, independent of the change of E. The AR numerical results are shown in Fig. 2 with $\Gamma = 0.5$. With respect to the effective pairing potentials in the QDs, they are assumed to be the same with $\Delta = 0.5$ and 0.25, respectively. First, Figs. 2(a)–2(c) correspond to the results of $\varepsilon_1 = 0$, 0.25, and 0.5, in the case of $\Delta = 0.5$. In Fig. 2(a) we see that the AR spectrum exhibits the symmetric structure about the axis of $E = 0$ and $\varepsilon_2 = 0$. And in the case of $\varepsilon_2 = 0$, the AR encounters its zero value. In addition, it shows that four peaks exist in the AR spectrum. The first and fourth peaks are notably narrow, and they tightly depend on the change of ε_2 or E. Instead, the other two peaks are hybridized seriously and their positions are relatively stationary. Figures 2(b) and 2(c) show that when the level of QD-1 shifts away from the zero energy point, the asymmetry of the AR spectrum becomes apparent with the change of ε_2. In the case of $\varepsilon_1 = 0.5$, the AR is almost suppressed in the region of $\varepsilon_2 > 0$, whereas in the region of $\varepsilon_2 < 0$, the AR is enhanced to a great degree. Besides, when $\varepsilon_2 < 0$, the second and third AR peaks almost get crossed, as a result, the AR becomes resonant around the position of $E = 0$. Next in Figs. 2(d)–2(f), when the superconducting pairing potentials in the QDs decrease to be $\Delta = 0.25$, the AR spectra are narrowed seriously and the AR phenomenon mainly occurs in the region of $|E| < 0.5$. Besides, the contributions of the first and fourth molecular states become more weak. The other result lies in that all the AR peaks are relatively ambiguous, especially for the peaks near the energy zero point. Therefore, compared with the case of single-electron tunneling, the AR peaks are related to the eigenlevels of the QDs in the Nambu representation in an alternative way, since no antiresonance phenomena depend on the variation of E.

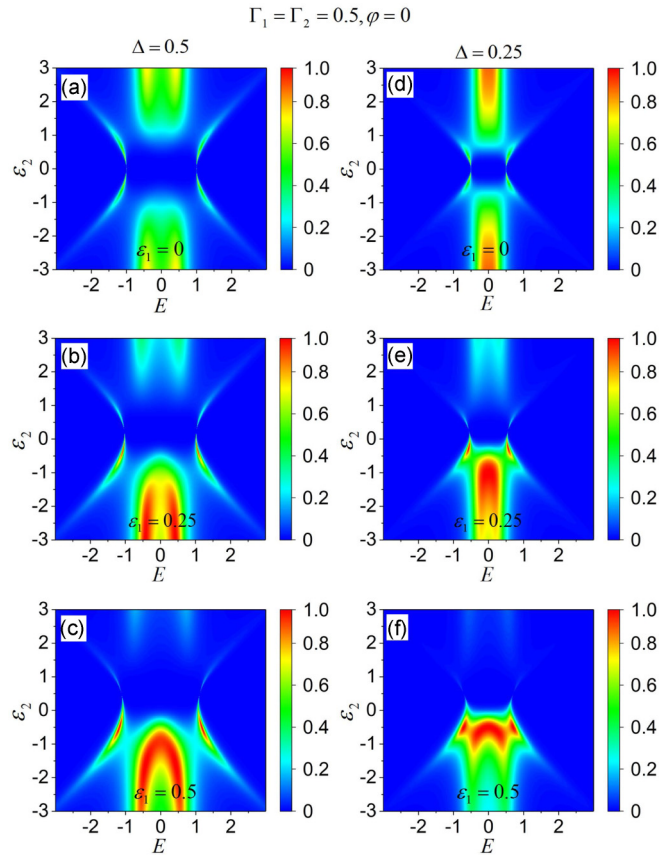

FIG. 2. AR spectra in the parallel double QD structure, in the case of identical QD-lead couplings with $\Gamma = 0.5$. The level of QD-1 is taken to be $\varepsilon_1 = 0$, 0.25, and 0.5, respectively. The results in (a)–(c) denote the cases of $\Delta = 0.5$, and (d)–(f) correspond to the results of $\Delta = 0.25$.

In Fig. 3 we introduce local magnetic flux through this ring junction to investigate the AR properties. From Eq. (17) it can be observed that in the case of $\varphi = \pi$, $\tau(E)$ has an opportunity to be equal to zero, corresponding to the occurrence of antiresonance at the positions of $E = \pm\frac{1}{2}(\varepsilon_1 + \varepsilon_2)$. Figures 3(a)–3(c) show the results of $\frac{\varphi=\pi}{3}, 2\pi$ and π, respectively, in the case of $\varepsilon_1 = 0.5$ with $\Delta = 0.5$. And the results of $\Delta = 0.25$ are exhibited in Figs. 3(d)–3(f). One can readily find that with the increase of magnetic flux, the AR spectrum experiences obvious changes. First, the first and fourth AR peaks are strengthened and widened apparently. On the other hand, the magnetic flux modifies the role of ε_2, and then no antiresonance comes into being [see Figs. 3(a) and 3(b)]. As shown in Fig. 3(c), when ε_2 changes in the positive-energy region, the AR begins to be more active. Besides, due to the occurrence of antiresonances, the edges of the respective parts of the AR spectrum can be clearly seen in the case of $\varphi = \pi$. Next for the case of $\Delta = 0.25$, the leading properties of the AR spectra are basically similar to those in the above case [see Figs. 3(d)–3(f)]. The difference is the narrowness of the AR spectra, which inevitably reregulates the AR peaks. As shown

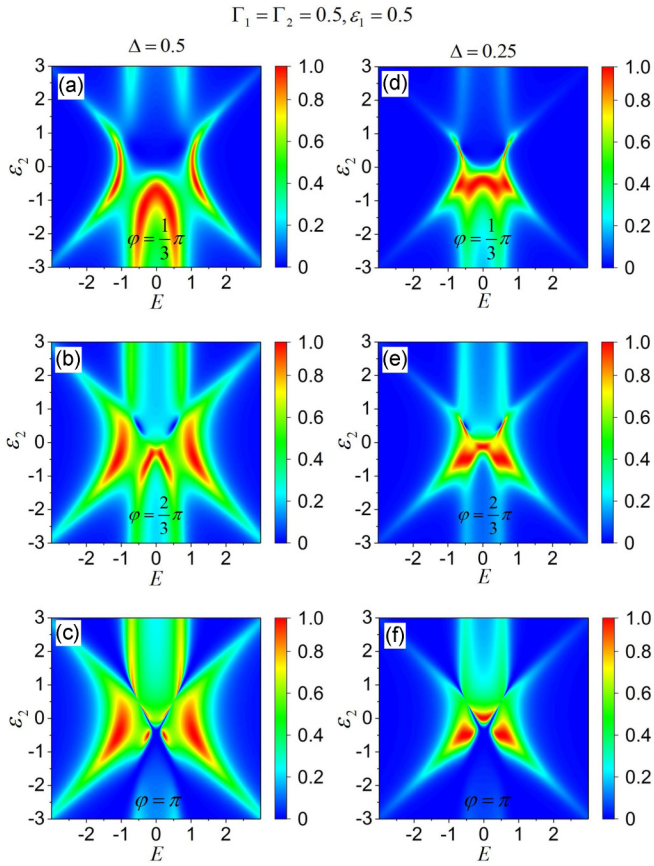

FIG. 3. AR spectra affected by the local magnetic flux through this system. The level of QD-1 is fixed with $\varepsilon_1 = 0.5$. And the other structural parameters are the same as those in Fig. 2, respectively.

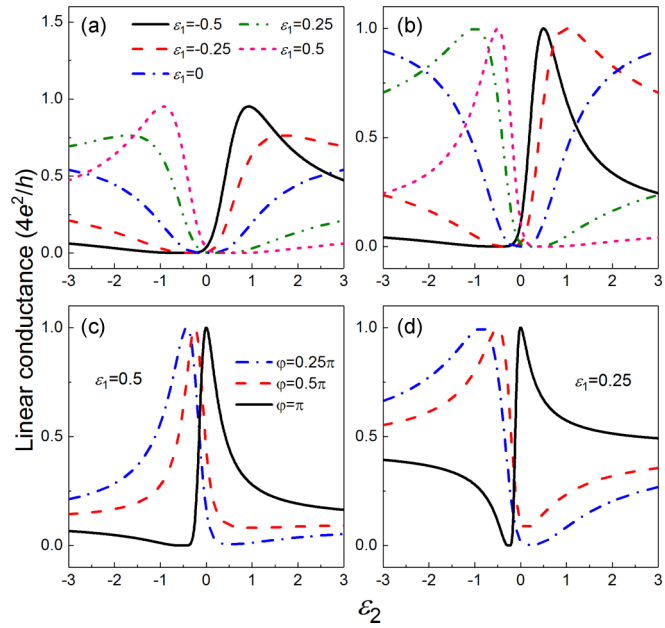

FIG. 4. Linear-conductance curves of the AR process in the parallel double QD structure. The QD-lead coupling strengths are $\Gamma = 0.5$. (a) and (b) Results in the cases of $\Delta = 0.5$ and 0.25, respectively. The level of QD-1 is taken to be $\varepsilon_1 = \pm 0.5$, ± 0.25, and 0. (c) and (d) Influence of magnetic flux on the linear AR conductance when $\Delta = 0.25$.

in Fig. 3(f), only three peaks survive in the AR spectrum in the case of $\varphi = \pi$.

Motivated by the intricate results of AR, we would like to focus on its linear conductance spectrum to further clarify the AR property. According to Eq. (14), the linear conductance is related to the AR transmittance in the case of $E = 0$. In Fig. 4 we plot the linear conductance curves, by taking $\Delta = 0.5$ and 0.25, respectively. First, Fig. 4(a) shows the results of the fixed level of QD-1, where $\varepsilon_1 = \pm 0.5$, ± 0.25, and 0. We can clearly find that in the case of $\varepsilon_1 = 0.5$, the Fano line shape appears in the linear conductance spectrum, with the Fano peak and antiresonance at the positions of $\varepsilon_2 = 0$ and $\varepsilon_2 = 1.0$. When the level of QD-1 shifts to $\varepsilon_1 = -0.5$, the Fano line shape is reversed. This suggests that in the linear AR process of the parallel double QD structure, Fano interference is allowed to take place, and its mode can be adjusted with the electric method. If we choose $\varepsilon_1 = \pm 0.25$, there also exist the Fano line shapes in the conductance spectra. However, no Fano resonance peak exists in such cases. When $\varepsilon_1 = 0$, only one symmetric line shape can be observed, despite the occurrence of antiresonance at the position of $\varepsilon_2 = 0.5$. Next, if Δ decreases to 0.25, one can find from Fig. 4(b) that the Fano resonance is allowed to appear as well, independent of the change of ε_1. Therefore, the effective pairing potentials in the QDs play their special roles in driving the Fano resonance in the linear AR process. In addition, as shown in Figs. 4(c) and 4(d), the local magnetic flux can effectively modify the Fano line shape in the conductance spectrum. Until $\varphi = \pi$, the Fano line shape is reversed. Note, however, that differently from the electric tuning [47], the Fano peak in the case of $\varphi = \pi$ becomes narrow after the reversal of the Fano line shape.

B. Case of asymmetric coupling

In this part we would like to pay attention to the case of asymmetric QD-lead(SC) coupling. One reason is that the quantum transport properties in the parallel double QD structure tightly depend on the QD-lead coupling manners. Without loss of generality, the QD-lead(SC) couplings are taken to be $\frac{\Gamma_1}{\Gamma_2} = \frac{\Delta_1}{\Delta_2} = \lambda$, thus

$$\tau(E) = \frac{(1-\lambda)^2 E^2 - (\lambda\varepsilon_1 - \varepsilon_2)^2}{\det|[G^r(E)]^{-1}|}\Gamma_2\Delta_2 \qquad (18)$$

in the absence of magnetic flux. As a result, the antiresonances shift to the points of $E = \pm\frac{\lambda\varepsilon_1-\varepsilon_2}{1-\lambda}$.

Figure 5 shows the AR spectra in the cases of $\Delta_1 = 1.0$ and 0.5, respectively, by taking the magnetic flux out of account. With respect to the value of λ, it is chosen to be $\lambda = 10$. We see that the asymmetry of the QD-lead couplings has the nontrivial effect on the AR process of this case. First, in Fig. 5(a) it shows that with the change of E, two main peaks appear in the AR spectrum, near the regions of $E = \pm 1.0$. The positions of the AR peaks seem to be independent of the shift of ε_2. The other phenomenon is that the AR spectrum is clearly divided into four regions by the two antiresonance conditions shown in the above paragraph. Accordingly, the value of $T_A(E)$ is exactly equal to zero at the energy zero point.

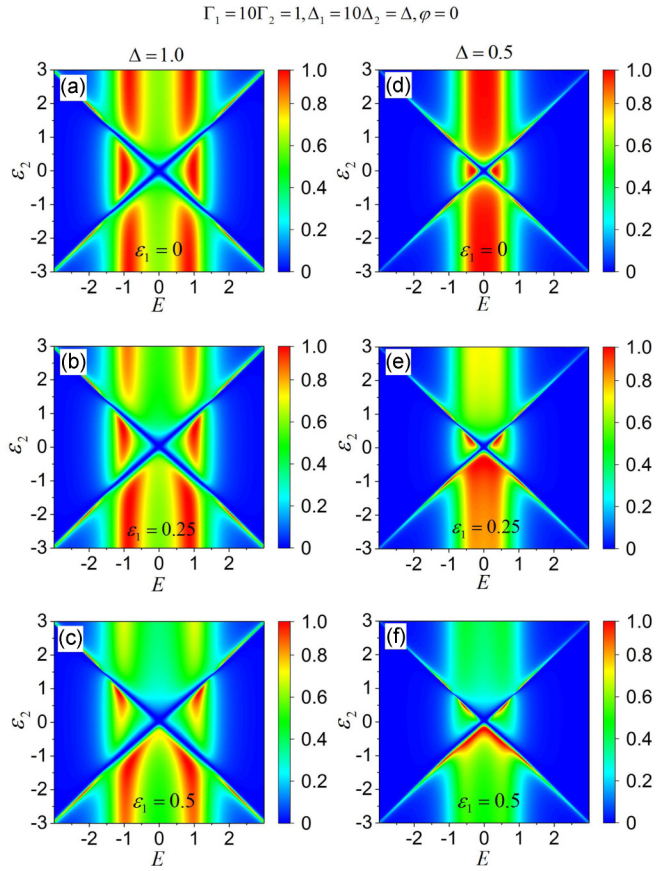

FIG. 5. AR spectra of the parallel double QD structure when $\varepsilon_1 = 0$, 0.25, and 0.5, respectively. The QD-lead coupling strength is $\Gamma_1 = 10\Gamma_2 = 1.0$. (a)–(c) Results in the case of $\Delta_1 = 1.0$; (d)–(f) those of $\Delta_1 = 0.5$.

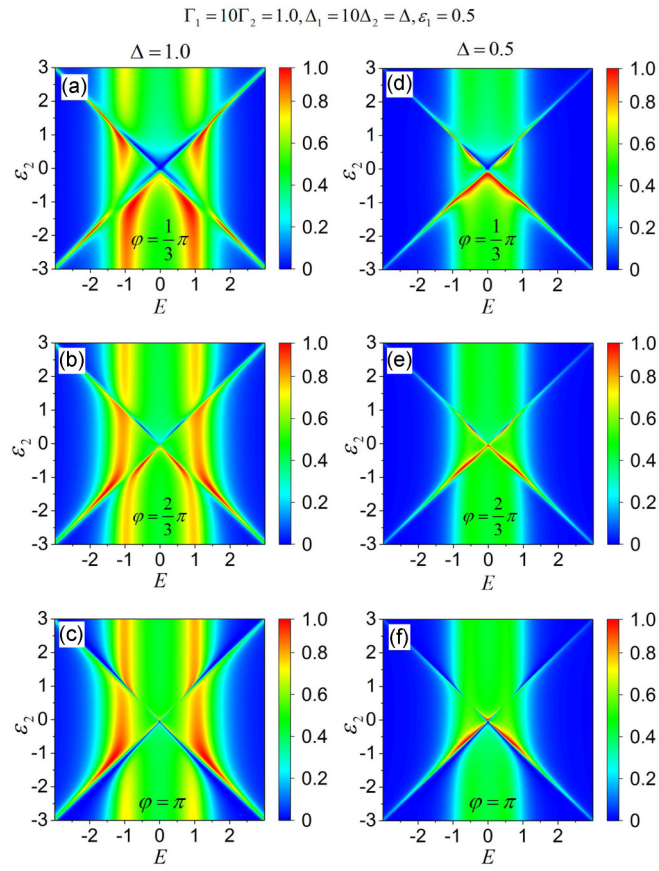

FIG. 6. AR spectra affected by the local magnetic flux through this system. ε_1 is assumed to be 0.5. The other parameters are identical with those in Fig. 7, respectively.

With the increase of ε_1, the asymmetric AR spectrum comes into being with the shift of ε_2, as shown in Figs. 5(b) and 5(c). Meanwhile, the edges of the four AR regions get to be unclear gradually, though the lines are not modified obviously by the change of ε_2. Next, the case of $\Delta_1 = 0.5$ is exhibited in Figs. 5(d)–5(f). In the situation of $\varepsilon_1 = 0$, one can find one wide peak around the point of $E = 0$. With the increase of ε_1, this peak is destroyed, and the suppression of the AR process can also be observed, accompanied by the appearance of the asymmetric AR spectrum. Therefore, the asymmetry of the QD-lead coupling can efficiently alter the AR properties in our considered structure.

In Fig. 6 we present the influence of the local magnetic flux through this ring on the AR properties. Figures 6(a)–6(c) show the results of $\frac{\varphi=\frac{\pi}{3}, 2\pi}{3}$ and π, respectively, in the case of $\varepsilon_1 = 0.5$ with $\Delta_1 = 1.0$. And Figs. 6(d)–6(f) correspond to the result of $\Delta_1 = 0.5$. In this figure one can find that with the increase of magnetic flux, the AR spectrum exhibits obvious changes. Similar to the results in Fig. 3, the first AR peak is strengthened and widened apparently. In addition, the AR maximum near the positions of $E = \pm 1.0$ is suppressed, compared with the case of $\varphi = 0$. The other result is that due to the disappearance of antiresonances, the boundaries of the AR spectrum become ambiguous in the cases of $\varphi = \frac{\pi}{3}$ and $\frac{2\pi}{3}$. Next, Figs. 6(d)–6(f) show that the magnetic flux indeed reverses the symmetry of the AR spectrum, but the AR transmittance cannot be enhanced in this process.

The results in Figs. 5 and 6 show that the antiresonance is allowed to take place even in the case of $E = 0$ when $\varphi = n\pi$. Thus we anticipate that the Fano effect can be observed in the linear conductance spectrum despite the asymmetry of the QD-lead couplings. With this idea, we plot the linear conductance profile of the AR in Fig. 7. It is clearly shown that apparent Fano line shapes exist in the linear AR conductance spectra. As shown in Figs. 7(a) and 7(b), the Fano effect is enhanced when the superconducting pairing potentials in the QDs decrease to be $\Delta = 0.5$. This is due to the fact that in this case, the Fano resonance is able to occur. Also, in comparison with the result in Fig. 4, the reference channel makes more contribution to the Fano effect in this case, because of the increase of the conductance value outside the Fano interference region. In addition, Figs. 7(c) and 7(d) show that the local magnetic flux can reverse the Fano line shape in the conductance spectrum. Up to now, we have known that in this structure, the Fano effect is robust in the linear AR process when one arm provides the reference channel.

C. Analysis on the Fano effect

We next aim to clarify the Fano effect in the linear AR process. It is well known that for discussing the Fano effect, one has to transform the conductance expression into its Fano

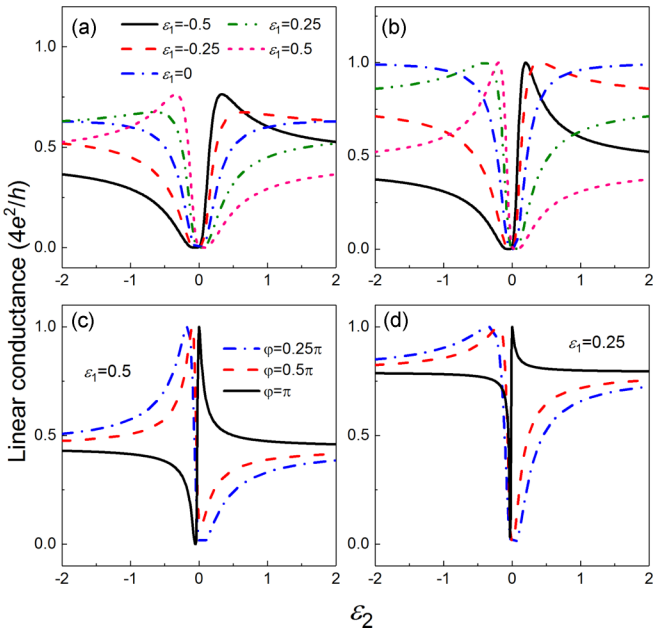

FIG. 7. Linear AR conductance in the parallel double QD structure with the change of the structural parameters. (a) and (b) Results in the cases of $\Delta_1 = 1.0$ and 0.5. And the level of QD-1 is taken to be $\varepsilon_1 = \pm 0.5, \pm 0.25$, and 0. (c) and (d) Impact of magnetic flux on the conductance spectra.

form. Hence, we start to analyze the Fano effect in the linear AR process by presenting the analytical expression of the AR coefficient. After deduction, we are allowed to obtain the Fano expression of $\tau|_{E=0}$, i.e., $\tau|_{E=0} = \tau_b \frac{\alpha(e+q)^2}{\alpha e^2+1} e^{i\varphi}$ (see Appendix C). And then,

$$T_A|_{E=0} = |\tau_b|^2 \frac{\alpha^2 |e+q|^4}{|\alpha e^2+1|^2}. \tag{19}$$

Here $\tau_b = \frac{4\Gamma_1\Delta_1}{4\varepsilon_1^2+\Gamma_1^2+4\Delta_1^2}$ is the AR coefficient in the absence of QD-2. One can understand that when the level of QD-1 is fixed but not equal to zero, the arm of QD-1 enables us to provide the reference channel for the Fano interference in the linear AR process. Next, $e = \varepsilon_2 + \tau_b \frac{\Gamma_1\Gamma_2+4\Delta_1\Delta_2}{4\Gamma_1\Delta_1}\varepsilon_1$, and

$$q = -\left(\frac{\Gamma_1\Gamma_2+4\Delta_1\Delta_2}{4\Gamma_1\Delta_1}\tau_b + \frac{\sqrt{\Gamma_2\Delta_2}}{\sqrt{\Gamma_1\Delta_1}}e^{-i\varphi}\right)\varepsilon_1 \tag{20}$$

is the so-called Fano parameter. In addition, it shows that the other quantity also comes into play, i.e., $\alpha = \frac{16\Gamma_1^2\Delta_1^2}{[4\varepsilon_1^2(\Gamma_1\Delta_2-\Delta_1\Gamma_2)^2+4\varepsilon_1^4(\Gamma_2^2+4\Delta_2^2)]\tau_b^2+4\Gamma_1\Delta_1\tau_b C}$, which is always positive. It should be noticed that this Fano expression is basically complicated and different from the result in the case of single electron tunneling where $T_{et} = T_b \frac{|e+q|^2}{e^2+1}$ with T_b being the electron tunneling ability in the reference channel [47,54,55]. This indicates the complicated characteristic of the Fano effect in the linear AR process.

As shown in Eq. (19), although the AR contributed by QD-1 can provide the reference channel, the information of the resonance channel cannot be directly obtained from the other arm, due to the complexity of the parameter e. Surely, with the change of e, the profile of $T_A|_{E=0}$ indeed exhibits the Fano line shape, for a real Fano parameter q. And when the sign of q (i.e., $\pm$) changes, the Fano line shape will be reversed. One can then understand the Fano line shapes in the linear conductance spectra in Figs. 4 and 7. The Fano antiresonance can be analyzed as follows. When finite magnetic flux is introduced through this ring, the Fano parameter q will become complex, so $e + q \neq 0$ and the Fano effect will be suppressed. Otherwise, in the cases of $\varphi = 0$ or $\varphi = \pi$, the positions of the Fano antiresonances can be ascertained by letting $e + q = 0$, and the corresponding conditions can be solved, i.e.,

$$\varepsilon_1\sqrt{\Gamma_2\Delta_2} \mp \varepsilon_2\sqrt{\Gamma_1\Delta_1} = 0. \tag{21}$$

This relationship is simplified to be $\varepsilon_1 \mp \varepsilon_2 = 0$ in the case of $\Delta_j = \Delta$ with the identical QD-lead couplings. According to these results, we know that for a fixed ε_1, the antiresonance points always exist in the linear conductance spectra, with their positions being at the points of $\varepsilon_2 = \pm\sqrt{\frac{\Gamma_2\Delta_2}{\Gamma_1\Delta_1}}\varepsilon_1 = \pm\lambda\varepsilon_1$ in the case of $\varphi = 0$ or $\varphi = \pi$.

It should be emphasized that the Fano interference is determined by the eigenlevels of the QD molecule and the molecule-lead(SC) couplings in the Nambu representation [see Fig. 1(b)]. In order to present a clear description, we would like to calculate the eigenlevels of the QD molecule with finite molecule-lead(SC) couplings. The effective Hamiltonian matrix can be given by

$$\mathcal{H} = \begin{bmatrix} \varepsilon_1 - \frac{i}{2}\Gamma_{11,e} & -\Delta_1 & -\frac{i}{2}\Gamma_{12,e} & \sqrt{\Delta_1\Delta_2} \\ -\Delta_1 & -\varepsilon_1 - \frac{i}{2}\Gamma_{11,e} & \sqrt{\Delta_1\Delta_2} & -\frac{i}{2}\Gamma_{12,h} \\ -\frac{i}{2}\Gamma_{21,e} & \sqrt{\Delta_1\Delta_2} & \varepsilon_2 - \frac{i}{2}\Gamma_{22,e} & -\Delta_2 \\ \sqrt{\Delta_1\Delta_2} & -\frac{i}{2}\Gamma_{21,h} & -\Delta_2 & -\varepsilon_2 - \frac{i}{2}\Gamma_{22,h} \end{bmatrix}.$$

The spectra of the eigenlevels are shown in Fig. 8. Figures 8(a)–8(d) describe the result of $\Delta_j = \Delta$ and $\Gamma_j = \Gamma$. As for the QD levels, we take $\varepsilon_1 = 0$ and $\varepsilon_1 = 0.5$, respectively. It is readily found that if $\Gamma = 0$, the analytical expressions of E_j can be written out, i.e., $E_1 = -E_4 = \frac{-1}{\sqrt{2}}\sqrt{\varepsilon_1^2+\varepsilon_2^2+4\Delta^2+\Omega}$ and $E_2 = -E_3 = \frac{-1}{\sqrt{2}}\sqrt{\varepsilon_1^2+\varepsilon_2^2+4\Delta^2-\Omega}$ with $\Omega = \sqrt{(\varepsilon_1^2-\varepsilon_2^2)^2+4\Delta^2(\varepsilon_1-\varepsilon_2)^2+16\Delta^4}$. They are consistent with the results in Figs. 8(a) and 8(b). Thus, the QD-lead coupling only contributes to the imaginary parts of the eigenlevels, as shown in Figs. 8(c) and 8(d). By observing the results of the eigenlevels, we can explain the leading feature of the linear AR conductances from the following two aspects. First, the symmetry of the conductance curves is determined by the eigenlevel spectra with the change of ε_2. In

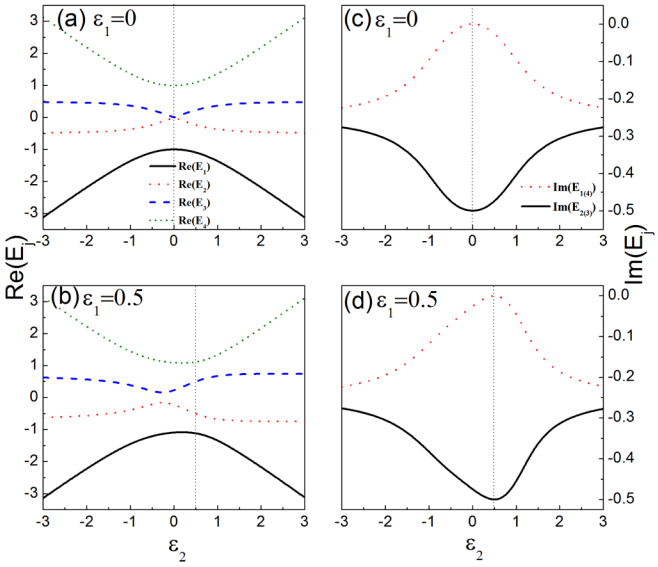

FIG. 8. Eigenlevels of the double QDs in the Nambu representation, due to their coupling with the normal lead and SC. The parameters are taken to be $\Gamma_j = \Gamma = 1.0$ and $\Delta_j = \Delta = 0.5$. (a) and (b) Real parts of the eigenlevels in the cases $\varepsilon_1 = 0$ and $\varepsilon_1 = 0.5$. (c) and (d) Corresponding imaginary parts.

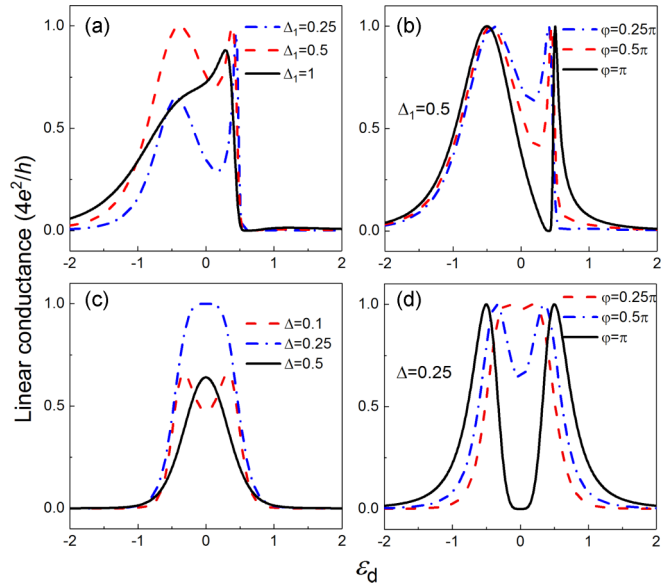

FIG. 9. Linear conductance of the AR in the cases of $\varepsilon_j = \varepsilon_d \pm \delta$ with $\delta = 0.5$. (a) and (b) Results of $\Gamma_1 = 10\Gamma_2$ and $\Delta_1 = 10\Delta_2$. (c) and (d) Case of identical QD-lead(SC) couplings, i.e., $\Gamma_j = \Gamma$ and $\Delta_j = \Delta$.

the case of $\varepsilon_1 = 0.5$, the maximum of E_2 shifts to the position of $\varepsilon_2 = -0.25$, and the maximum of E_1 shifts to $\varepsilon_2 = 0.25$. Meanwhile, $|\mathrm{Re}(E_3 - E_2)|_{\varepsilon_2 < -0.25} < |\mathrm{Re}(E_4 - E_1)|_{\varepsilon_2 > -0.25}$, and a similar result can be observed between E_1 and E_4 beside the point of $\varepsilon_2 = 0.25$. One can then understand the asymmetric line shape of the linear AR conductance. Second, with respect to the antiresonance, it certainly originates from the destructive quantum interference among the channels formed by the coupling between the molecular states and lead-e (lead-h). The analysis shows that the AR coefficient can be expressed as the superposition of four Feynman paths, i.e., $\tau(E) = \sum_j \mathcal{P}_j$ with $\mathcal{P}_j = \frac{(-1)^j \mathrm{Im}E_j}{E - \mathrm{Re}E_j - i\mathrm{Im}E_j}$. $\mathcal{P}_j$ is exactly the direct product of the Green function and eigenlevel widening of the jth molecular state. In Figs. 8(c) and 8(d) we see that around the antiresonance position, the imaginary parts of E_1 and E_4 get close to zero, so their contributed paths do not influence the quantum interference. And then, the antiresonance point in the linear conductance spectrum is mainly determined by the interference between $\mathcal{P}_2$ and $\mathcal{P}_3$. When $\varepsilon_2 = 0.5$, the imaginary parts of E_2 and E_3 reach their maxima, leading to the enhancement of destructive quantum interference.

Since the Fano interference can be achieved when the two arms provide the reference and resonance channels, respectively, we would like to investigate the case where the levels of the two QDs are shiftable, e.g., $\varepsilon_1 = \varepsilon_d + \delta$ and $\varepsilon_2 = \varepsilon_d - \delta$ by taking $\Gamma_1 = 10\Gamma_2$ and $\Delta_1 = 10\Delta_2$. One expects that the Fano effect can be driven, due to the asymmetric QD-lead coupling in this situation. As shown in Fig. 9(a), when $\Delta_1 = 0.25$, two peaks appear in the linear-conductance spectrum. One is "more" resonant and the other is "less" resonant. This is exactly the necessary condition of the Fano interference and gives rise to the Fano effect. When $\Delta_1 = 0.5$, the conductance magnitude increases, and the Fano effect becomes apparent. However, the further increase of Δ_1 can only weaken the Fano effect (see the case of $\Delta = 1.0$). Next, applying the magnetic flux with $\varphi = \pi$ reverses the Fano line shape in the conductance spectrum, as shown in Fig. 9(b). We can then find that even when the two QDs are both level tunable, the Fano effect can also be induced in the linear AR process, in the presence of the asymmetric QD-lead couplings.

For comparison, in Figs. 9(c) and 9(d) we present the other case, i.e., $\Gamma_j = \Gamma$ and $\Delta_j = \Delta$, by considering $\varepsilon_1 = \varepsilon_d + \delta$ and $\varepsilon_2 = \varepsilon_d - \delta$ with $\delta = 0.5$. As shown in Fig. 9(c), two peaks appear in the linear-conductance spectrum in the case of $\Delta = 0.1$. With the increase of Δ to $\Delta = 0.25$, one peak arises at the position of $\varepsilon_d = 0$ in the conductance spectrum. When Δ is further increased to be $\Delta = 0.5$, the conductance peak is weakened. Thus in such a case, no Fano effect takes place. The underlying physics should be attributed to the disappearance of the reference channel. When the magnetic flux is taken into account, the conductance spectrum can be changed, as shown in Fig. 9(d). In the case of $\varphi = \pi$, one antiresonance point can be observed at the position of $\varepsilon_d = 0$, but it cannot be viewed as the Fano antiresonance.

D. Effect of Coulomb interaction in the QDs

Before concluding, it is necessary for us to make a remark regarding the many-body effect which we have by far ignored. However, the many-body effect is an important origin for the peculiar transport properties in the QD-based structures, including the ARs. Therefore, it is supposed to influence the Fano effect in a substantial way. Usually, the many-body effect is incorporated by only considering the intradot Coulomb repulsion, i.e., the Hubbard term $H_{ee} = \sum_j U_j n_{j\uparrow} n_{j\downarrow}$. In this work we would like to describe the influence of Coulomb interaction on the Fano effect in the linear AR process by taking the Hubbard term into account.

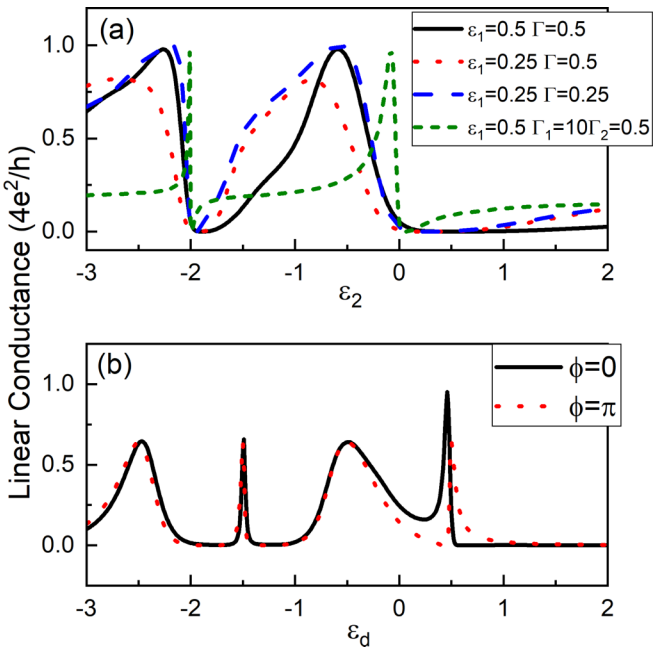

FIG. 10. Linear AR conductance in the case of finite Coulomb interaction with $U_j = U = 2.0$. (a) Results of fixed ε_1. (b) Conductance curves in the case of $\varepsilon_{1(2)} = \varepsilon_d \pm \delta$. Other parameters are the same as those in Figs. 9(a) and 9(b).

If the Hubbard interaction is not very strong, we can truncate the equations of motion of the Green functions within the Hubbard-I approximation [56,57]. By a straightforward derivation, we find that the theoretical description and the relevant results developed above are still valid. The only difference consists in the change of $g_{je,\sigma} = [\frac{(z-\varepsilon_j)(z-\varepsilon_j-U_j)}{z-\varepsilon_j-U_j+U_j\langle n_{j\bar{\sigma}}\rangle} + \frac{i}{2}\Gamma_{jj,e}]^{-1}$ and $g_{jh,\sigma} = [\frac{(z+\varepsilon_j)(z+\varepsilon_j+U_j)}{z+\varepsilon_j+U_j-U_j\langle n_{j\bar{\sigma}}\rangle} + \frac{i}{2}\Gamma_{jj,h}]^{-1}$ with $z = E + i0^+$. $\langle n_{j\sigma}\rangle$ is the average occupation of the spin-σ electron in QD-j, and it can be defined as $\langle n_{j\sigma}\rangle = -\frac{1}{\pi}\int dE[\mathrm{Im}G^r_{jj,\sigma}(E)]$. The linear conductance spectra of $U_j = U = 2.0$ are shown in Fig. 10. It can be found that due to the many-body effect, the main variation in the linear conductance spectra is manifested as the appearance of two Fano antiresonances. For the case of fixed ε_1, two antiresonance points emerge in the conductance curves with the adjustment of ε_2, as exhibited in Fig. 10(a). And around the antiresonance points, the Fano line shapes can be clearly observed. Next in Fig. 10(b) where $\varepsilon_{1(2)} = \varepsilon_d \pm \delta$, we see that the intradot Coulomb interaction is also able to induce the two-group splitting of the conductance spectra. However, the conductance magnitude is suppressed by the existence of Coulomb interaction, and only the Fano line shape in the high-energy group is relatively noticeable. We would like to explain these phenomena as follows. Within the Hubbard-I approximation, the Coulomb interaction splits each QD level into two, i.e., ε_j and $\varepsilon_j + U_j$. Any levels close to the energy zero point will make leading contribution to the Fano interference. Therefore, the Fano line shapes in the conductance spectrum are doubled. In addition, due to the breaking of the electron-hole symmetry in this system, the Fano line shapes in the two groups are different from each other, especially for the results in Fig. 10(b).

If the electron interaction is very strong, the electron correlation effect should be taken into account. One needs to extend the theoretical treatment by adding the interdot interaction and beyond the Hubbard-I approximation. And then, the further modification to the Fano line shapes will naturally arise. It is known that the renormalization group (NRG) method seems to be a better approach to treat the many-body effect in the electron-correlation regime [58]. Such an interesting issue will be discussed in future studies.

IV. SUMMARY

In summary, in this work we have built the heterostructure of a metallic lead coupled to one s-wave SC via the QDs and comprehensively studied the AR properties in the parallel double QD system. As a result, it has been found that Fano line shapes will appear in the linear conductance spectra of the AR process, if an arm of this setup plays the role of the reference channel for the quantum interference. And similar to the single-electron transport, the Fano line shapes can be reversed by adjusting the QD level or local magnetic flux. However, the characteristic of the Fano resonance is completely different from that in the single-electron transport case. In order to clarify the underlying reason for this kind of Fano effect, we have first obtained the Fano form of the linear-conductance expression, and then we have presented detailed descriptions about the Fano effect. Moreover, the underlying Fano interference mechanism has been clarified by discussing the molecular states in the presence of QD-lead(SC) couplings. We believe that the results of this work can enrich the meaning of the Fano interference.

ACKNOWLEDGMENTS

W.-J.G. thanks Zhi-Qiang Bao and Yi-Song Zheng for helpful discussions. This work was financially supported by the Liaoning BaiQianWan Talents Program (Grant No. 201892126) and the Fundamental Research Funds for the Central Universities (Grants No. N170506007 and No. N182410008-1).

APPENDIX A: EFFECTIVE FORM OF THE HAMILTONIAN THE QDS COUPLED TO ONE SC

For the system with two QDs coupled through one s-wave SC, the Green's function matrix can be written as

$$[G^r(E)]^{-1} = \begin{bmatrix} \omega-\varepsilon_1-\Sigma^{11}_{ee} & -\Sigma^{11}_{eh} & -\Sigma^{12}_{ee} & -\Sigma^{12}_{eh} \\ -\Sigma^{11}_{he} & \omega+\varepsilon_1-\Sigma^{11}_{hh} & -\Sigma^{12}_{he} & -\Sigma^{12}_{hh} \\ -\Sigma^{21}_{ee} & -\Sigma^{21}_{eh} & \omega-\varepsilon_2-\Sigma^{22}_{ee} & -\Sigma^{22}_{eh} \\ -\Sigma^{21}_{he} & -\Sigma^{21}_{hh} & -\Sigma^{22}_{he} & \omega+\varepsilon_2-\Sigma^{22}_{hh} \end{bmatrix} \quad \text{(A1)}$$

in the basis $\{d_{1\uparrow}^\dagger, d_{1\downarrow}, d_{2\uparrow}^\dagger, d_{2\downarrow}\}$. The self-energy is defined as $\Sigma = \sum_k H_{D,sk} g_{sk} H_{sk,D}$ with g_{sk} being the Green's function of the isolated SC. In the basis $\{a_{k\uparrow}^\dagger, a_{k\downarrow}\}$, $g_{sk} = \begin{bmatrix} \omega-\epsilon_k & -\Delta_k \\ -\Delta_k & \omega+\epsilon_k \end{bmatrix}^{-1}$. And then, $H_{D,sk} = H_{D,sk}^\dagger = \begin{bmatrix} W_{1k} & 0 & W_{2k} & 0 \\ 0 & -W_{1k}^* & 0 & -W_{2k}^* \end{bmatrix}$.

Via derivation, the self-energy can be expressed in the energy space, i.e.,

$$\Sigma = \begin{bmatrix} -i\Delta_1\beta(\omega) & -i\Delta_1\beta(\omega)\frac{\Delta}{\omega} & -i\sqrt{\Delta_1\Delta_2}\beta(\omega) & i\sqrt{\Delta_1\Delta_2}\beta(\omega)\frac{\Delta}{\omega} \\ -i\Delta_1\beta(\omega)\frac{\Delta^*}{\omega} & -i\Delta_1\beta(\omega) & i\sqrt{\Delta_1\Delta_2}\beta(\omega)\frac{\Delta}{\omega} & -i\sqrt{\Delta_1\Delta_2}\beta(\omega) \\ -i\sqrt{\Delta_1\Delta_2}\beta(\omega) & i\sqrt{\Delta_1\Delta_2}\beta(\omega)\frac{\Delta}{\omega} & -i\Delta_2\beta(\omega) & -i\Delta_2\beta(\omega)\frac{\Delta}{\omega} \\ i\sqrt{\Delta_1\Delta_2}\beta(\omega)\frac{\Delta}{\omega} & -i\sqrt{\Delta_1\Delta_2}\beta(\omega) & -i\Delta_2\beta(\omega)\frac{\Delta}{\omega} & -i\Delta_2\beta(\omega) \end{bmatrix}, \tag{A2}$$

where $\beta(\omega) = \frac{|\omega|\theta(|\omega|-|\Delta|)}{\sqrt{\omega^2-|\Delta|^2}} + \frac{\omega\theta(|\Delta|-|\omega|)}{i\sqrt{|\Delta|^2-\omega^2}}$. $\Delta_j = \pi|W_j|^2\rho_s$ with ρ_s being the density of state of the quasiparticle in the SC. And W_j has been assumed to be real. Note that Σ_{eh}^{jj} and $\Sigma_{eh}^{jj'}$ correspond to the local AR and crossed AR terms, respectively. Since the fermionic operators obey the relationship of the exchange antisymmetry, they differ from each other by a minus sign [59].

In the limit of $|\Delta| \to \infty$, $\beta(\omega) = \frac{\omega}{i\sqrt{|\Delta|^2-\omega^2}}$, and then we have

$$\Sigma = \begin{bmatrix} 0 & -\Delta_1 & 0 & \sqrt{\Delta_1\Delta_2} \\ -\Delta_1 & 0 & \sqrt{\Delta_1\Delta_2} & 0 \\ 0 & \sqrt{\Delta_1\Delta_2} & 0 & -\Delta_2 \\ \sqrt{\Delta_1\Delta_2} & 0 & -\Delta_2 & 0 \end{bmatrix}. \tag{A3}$$

As a result,

$$\tilde{H}_d = \sum_{\sigma,j=1}^{2} \varepsilon_j d_{j\sigma}^\dagger d_{j\sigma} - \sum_{j=1}^{2} \Delta_j d_{j\uparrow}^\dagger d_{j\downarrow}^\dagger + \sqrt{\Delta_1\Delta_2} d_{1\uparrow}^\dagger d_{2\downarrow}^\dagger + \sqrt{\Delta_1\Delta_2} d_{2\uparrow}^\dagger d_{1\downarrow}^\dagger + \text{H.c.} \tag{A4}$$

Such a result indicates that the AR between the *s*-wave SC and QDs induces *s*-wave pairing potentials in the QDs, which is exactly the so-called the proximity effect.

APPENDIX B: SOLUTION OF GREEN'S FUNCTIONS

According to Eq. (7), we are able to obtain the expressions of respective Green's functions, i.e.,

$$\begin{aligned}
G_{12}^r &= -\frac{\Delta_1\big(E-\varepsilon_2+\frac{i}{2}\Gamma_2\big)\big(E+\varepsilon_2+\frac{i}{2}\Gamma_2\big) - \frac{\Gamma_1\Gamma_2}{4}\Delta_2 e^{-2i\varphi} + \frac{i}{2}\sqrt{\Delta_1\Delta_2\Gamma_1\Gamma_2}(2E+i\Gamma_2)e^{-i\varphi}}{\det|[G^r(E)]^{-1}|}, \\
G_{14}^r &= \frac{\sqrt{\Delta_1\Delta_2}\big[\big(E+\varepsilon_1+\frac{i}{2}\Gamma_1\big)\big(E-\varepsilon_2+\frac{i}{2}\Gamma_2\big) - \frac{\Gamma_1\Gamma_2}{4}\big] + \frac{i}{2}\sqrt{\Gamma_1\Gamma_2}\big[\big(E+\varepsilon_1+\frac{i}{2}\Gamma_1\big)\Delta_2 e^{-i\varphi} + \big(E-\varepsilon_2+\frac{i}{2}\Gamma_2\big)\Delta_1 e^{i\varphi}\big]}{\det|[G^r(E)]^{-1}|}, \\
G_{32}^r &= \frac{\sqrt{\Delta_1\Delta_2}\big[\big(E-\varepsilon_1+\frac{i}{2}\Gamma_1\big)\big(E+\varepsilon_2+\frac{i}{2}\Gamma_2\big) - \frac{\Gamma_1\Gamma_2}{4}\big] + \frac{i}{2}\sqrt{\Gamma_1\Gamma_2}\big[\big(E-\varepsilon_1+\frac{i}{2}\Gamma_1\big)\Delta_2 e^{-i\varphi} + \big(E+\varepsilon_2+\frac{i}{2}\Gamma_2\big)\Delta_1 e^{i\varphi}\big]}{\det|[G^r(E)]^{-1}|}, \\
G_{34}^r &= -\frac{\Delta_2\big(E-\varepsilon_1+\frac{i}{2}\Gamma_1\big)\big(E+\varepsilon_1+\frac{i}{2}\Gamma_1\big) - \frac{\Gamma_1\Gamma_2}{4}\Delta_1 e^{2i\varphi} + \frac{i}{2}\sqrt{\Delta_1\Delta_2\Gamma_1\Gamma_2}(2E+i\Gamma_1)e^{i\varphi}}{\det|[G^r(E)]^{-1}|},
\end{aligned} \tag{B1}$$

with $\det|[G^r(E)]^{-1}| = E^2[E+\frac{i}{2}(\Gamma_1+\Gamma_2)]^2 - E^2(\varepsilon_1^2+\varepsilon_2^2+\Delta_1^2+\Delta_2^2) - iE(\varepsilon_1^2\Gamma_2+\varepsilon_2^2\Gamma_1) - iE(\Gamma_1\Delta_2^2+\Gamma_2\Delta_1^2+\Gamma_1\Delta_1\Delta_2+\Gamma_2\Delta_1\Delta_2) - 2iE\sqrt{\Gamma_1\Gamma_2\Delta_1\Delta_2}(\Delta_1+\Delta_2)\cos\varphi + (\varepsilon_1\Gamma_2+\varepsilon_2\Gamma_1)^2 + 4(\varepsilon_1\Delta_2+\varepsilon_2\Delta_1)^2 + 4\varepsilon_1^2\varepsilon_2^2 + |\sqrt{\Gamma_1\Delta_2}e^{i\varphi/2} + \sqrt{\Gamma_2\Delta_1}e^{-i\varphi/2}|^4$.

APPENDIX C: FANO FORM OF AR TRANSMITTANCE

In Eq. (15),

$$\tau|_{E=0} = \frac{-4\big(e^{i\frac{\varphi}{2}}\varepsilon_2\sqrt{\Gamma_1\Delta_1} - e^{-i\frac{\varphi}{2}}\varepsilon_1\sqrt{\Gamma_2\Delta_2}\big)^2}{4\varepsilon_1^2\varepsilon_2^2 + (\varepsilon_1\Gamma_2+\varepsilon_2\Gamma_1)^2 + 4(\varepsilon_1\Delta_2+\varepsilon_2\Delta_1)^2 + \mathcal{C}} \tag{C1}$$

with $\mathcal{C} = |\sqrt{\Gamma_1\Delta_2}e^{i\varphi/2} + \sqrt{\Gamma_2\Delta_1}e^{-i\varphi/2}|^4$. Therefore, one can get the following result that

$$\tau|_{E=0} = -\tau_b \frac{e^{i\varphi}\big(\varepsilon_2 - e^{-i\varphi}\frac{\sqrt{\Gamma_2\Delta_2}}{\sqrt{\Gamma_1\Delta_1}}\varepsilon_1\big)^2}{\big(\varepsilon_2 + \frac{\Gamma_1\Gamma_2+4\Delta_1\Delta_2}{4\varepsilon_1^2+\Gamma_1^2+4\Delta_1^2}\varepsilon_1\big)^2 + \frac{1}{\alpha}}, \tag{C2}$$

where $\tau_b = \frac{4\Gamma_1\Delta_1}{4\varepsilon_1^2+\Gamma_1^2+4\Delta_1^2}$ and $\alpha = \frac{(4\varepsilon_1^2+\Gamma_1^2+4\Delta_1^2)^2}{4\varepsilon_1^2(\Gamma_1\Delta_2-\Delta_1\Gamma_2)^2+4\varepsilon_1^4(\Gamma_2^2+4\Delta_2^2)+(4\varepsilon_1^2+\Gamma_1^2+4\Delta_1^2)\mathcal{C}}$.

Next, by defining $e = \varepsilon_2 + \tau_b \frac{\Gamma_1\Gamma_2+4\Delta_1\Delta_2}{4\Gamma_1\Delta_1}\varepsilon_1$ and $q = -(\tau_b \frac{\Gamma_1\Gamma_2+4\Delta_1\Delta_2}{4\Gamma_1\Delta_1} e^{i\frac{\varphi}{2}} + \frac{\sqrt{\Gamma_2\Delta_2}}{\sqrt{\Gamma_1\Delta_1}} e^{-i\frac{\varphi}{2}})\varepsilon_1$, the Fano form of $\tau|_{E=0}$ can be written out, i.e.,

$$\tau|_{E=0} = -\tau_b \frac{\alpha(e+q)^2}{\alpha e^2+1} e^{i\varphi}. \tag{C3}$$

And then, the AR transmittance can be expressed as

$$T_A|_{E=0} = |\tau_b|^2 \frac{\alpha^2|e+q|^4}{|\alpha e^2+1|^2}. \tag{C4}$$

[1] U. Fano, Phys. Rev. **124**, 1866 (1961).
[2] A. E. Miroshnichenko, S. Flach, and Y. S. Kivshar, Rev. Mod. Phys. **82**, 2257 (2010).
[3] K. Kobayashi, H. Aikawa, S. Katsumoto, and Y. Iye, Phys. Rev. Lett. **88**, 256806 (2002); Phys. Rev. B **68**, 235304 (2003).
[4] J. Göres, D. Goldhaber-Gordon, S. Heemeyer, and M. A. Kastner, H. Shtrikman, D. Mahalu, and U. Meirav, Phys. Rev. B **62**, 2188 (2000).
[5] I. G. Zacharia, D. Goldhaber-Gordon, G. Granger, M. A. Kastner, Y. B. Khavin, H. Shtrikman, D. Mahalu, and U. Meirav, Phys. Rev. B **64**, 155311 (2001).
[6] M. Sato, H. Aikawa, K. Kobayashi, S. Katsumoto, and Y. Iye, Phys. Rev. Lett. **95**, 066801 (2005).
[7] K. Kobayashi, H. Aikawa, A. Sano, S. Katsumoto, and Y. Iye, Phys. Rev. B **70**, 035319 (2004).
[8] N. Myoung, J. W. Ryu, H. C. Park, S. J. Lee, and S. Woo, Phys. Rev. B **100**, 045427 (2019).
[9] L. S. Ricco, V. L. Campo Jr., I. A. Shelykh, and A. C. Seridonio, Phys. Rev. B **98**, 075142 (2018).
[10] B. R. Bułka and P. Stefański, Phys. Rev. Lett. **86**, 5128 (2001).
[11] W. Hofstetter, J. König, and H. Schoeller, Phys. Rev. Lett. **87**, 156803 (2001).
[12] B. Kubala and J. König, Phys. Rev. B **65**, 245301 (2002).
[13] A. Silva, Y. Oreg, and Y. Gefen, Phys. Rev. B **66**, 195316 (2002).
[14] D. I. Golosov and Y. Gefen, Phys. Rev. B **74**, 205316 (2006).
[15] V. Kashcheyevs, A. Schiller, A. Aharony, and O. Entin-Wohlman, Phys. Rev. B **75**, 115313 (2007).
[16] P. Y. Yang and W. M. Zhang, Phys. Rev. B **97**, 054301 (2018).
[17] K. Kang and S. Y. Cho, J. Phys.: Condens. Matter **16**, 117 (2004).
[18] Z. M. Bai, M. F. Yang, and Y. C. Chen, J. Phys.: Condens. Matter **16**, 4303 (2004).
[19] H. Lu, R. Lü, and B. F. Zhu, Phys. Rev. B **71**, 235320 (2005).
[20] M. L. Ladron de Guevara, F. Claro, and P. A. Orellana, Phys. Rev. B **67**, 195335 (2003).
[21] G. H. Ding, C. K. Kim, and K. Nahm, Phys. Rev. B **71**, 205313 (2005).
[22] H. Lu, R. Lü, and B. F. Zhu, J. Phys.: Condens. Matter **18**, 8961 (2006).
[23] K. Wrześniewski and I. Weymann, Phys. Rev. B **92**, 045407 (2015); W. J. Gong, Y. Han, G. Z. Wei, and A. Du, Nanoscale Res. Lett. **7**, 510 (2012).
[24] A. A. Clerk, X. Waintal, and P. W. Brouwer, Phys. Rev. Lett. **86**, 4636 (2001).
[25] W. J. Gong, C. Jiang, X. Sui, and A. Du, J. Phys. Soc. Jpn. **81**, 104601 (2012).
[26] T. Yamashita, S. Takahashi, and S. Maekawa, Phys. Rev. B **68**, 174504 (2003).
[27] J. Wang, Y. D. Wei, B. G. Wang, and H. Guo, Appl. Phys. Lett. **79**, 3977 (2001).
[28] Q. F. Sun, J. Wang, and T. H. Lin, Phys. Rev. B **59**, 3831 (1999).
[29] Y. Wei, J. Wang, H. Guo, H. Mehrez, and C. Roland, Phys. Rev. B **63**, 195412 (2001).
[30] Y. Zhu, T. H. Lin, and Q. F. Sun, Phys. Rev. B **69**, 121302(R) (2004).
[31] Z. M. Yu, Y. Liu, Y. Yao, and S. A. Yang, Phys. Rev. Lett. **121**, 176602 (2018).
[32] T. Sekera, C. Bruder, and R. P. Tiwari, Phys. Rev. B **98**, 195418 (2018).
[33] C. W. J. Beenakker, Rev. Mod. Phys. **69**, 731 (1997).
[34] T. Meng, J. Klinovaja, S. Hoffman, P. Simon, and D. Loss, Phys. Rev. B **92**, 064503 (2015).
[35] L. Hofstetter, S. Csonka, A. Baumgartner, G. Fülöp, S. d'Hollosy, J. Nygård, and C. Schönenberger, Phys. Rev. Lett. **107**, 136801 (2011).
[36] C. Bena, S. Vishveshwara, L. Balents, and M. P. A. Fisher, Phys. Rev. Lett. **89**, 037901 (2002).
[37] R. Mèlin and D. Feinberg, Eur. Phys. J. B **26**, 101 (2002).
[38] L. Li, Z. Cao, H. G. Luo, F. C. Zhang, and W. Q. Chen, Phys. Rev. B **92**, 195155 (2015).
[39] A. M. Calle, M. Pacheco, G. B. Martins, V. M. Apel, G. A. Lara, and P. A. Orellana, J. Phys.: Condens. Matter **29**, 135301 (2017).
[40] J. Peng, B. Wang, and D. Y. Xing, Phys. Rev. B **71**, 214523 (2005).
[41] J. L. Li and Y. X. Li, J. Phys.: Condens. Matter **20**, 465202 (2008).
[42] A. Kormányos, I. Grace, and C. J. Lambert, Phys. Rev. B **79**, 075119 (2009).
[43] Y. Tanaka, N. Kawakami, and A. Oguri, Phys. Rev. B **78**, 035444 (2008).
[44] J. Barański and T. Domański, Phys. Rev. B **85**, 205451 (2012).
[45] G. Fülöp, F. Domínguez, S. d'Hollosy, A. Baumgartner, P. Makk, M. H. Madsen, V. A. Guzenko, J. Nygård, C. Schönenberger, A. Levy Yeyati, and S. Csonka, Phys. Rev. Lett. **115**, 227003 (2015).
[46] F. Domínguez and A. Levy Yeyati, Physica E (Amsterdam) **75**, 322 (2016).
[47] W. Gong, Y. Zheng, Y. Liu, and T. Lü, Physica E (Amsterdam) **40**, 618 (2008).
[48] A. Fuhrer, P. Brusheim, T. Ihn, M. Sigrist, K. Ensslin, W. Wegscheider, and M. Bichler, Phys. Rev. B **73**, 205326 (2006).
[49] T. Domański, M. Žonda, V. Pokorný, G. Górski, V. Janiš, and T. Novotný, Phys. Rev. B **95**, 045104 (2017).

[50] A. Oguri, Y. Tanaka, and J. Bauer, Phys. Rev. B **87**, 075432 (2013).
[51] M. Governale, M. G. Pala, and J. König, Phys. Rev. B **77**, 134513 (2008).
[52] J. Eldridge, M. G. Pala, M. Governale, and J. König, Phys. Rev. B **82**, 184507 (2010).
[53] W. J. Gong, X. Q. Wang, Y. L. Zhu, and H. N. Wu, J. Appl. Phys. **119**, 214305 (2016).
[54] S. Wang, B. C. Lin, W. Z. Zheng, D. Yu, and Z. M. Liao, Phys. Rev. Lett. **120**, 257701 (2018).
[55] S. Norimoto, S. Nakamura, Y. Okazaki, T. Arakawa, K. Asano, K. Onomitsu, K. Kobayashi, and N. H. Kaneko, Phys. Rev. B **97**, 195313 (2018).
[56] J. Q. You and H. Z. Zheng, Phys. Rev. B **60**, 13314 (1999).
[57] X. Q. Wang, S. F. Zhang, Y. Han, G. Y. Yi, and W. J. Gong, Phys. Rev. B **99**, 195424 (2019).
[58] T. F. Fang, A. M. Guo, and Q. F. Sun, Phys. Rev. B **97**, 235115 (2018).
[59] Z. Scherübl, A. Pályi, and S. Csonka, Beilstein J. Nanotechnol. **10**, 363 (2019).